Materials Science for Energy Technologies 6 (2023) 484–492

Contents lists available at ScienceDirect

Materials Science for Energy Technologies

journal homepage: www.keaipublishing.com/en/journals/materials-science-for-energy-technologies

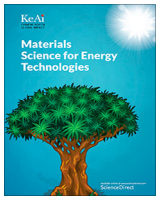

Insights into the influence of Pd loading on CeO_2 catalysts for CO_2 hydrogenation to methanol

Ramyakrishna Pothu [a], Harisekhar Mitta [b], Prasun Banerjee [c], Rajender Boddula [d,*], Rajesh K. Srivastava [e], Pramod K. Kalambate [f,g], Ramachandra Naik [h], Ahmed Bahgat Radwan [d], Noora Al-Qahtani [d,*]

[a] School of Physics and Electronics, College of Chemistry and Chemical Engineering, Hunan University, Changsha 410082, China
[b] Laboratory of Chemical Technologies, Ghent University, 9052 Zwaijnarde, Belgium
[c] Multiferroic and Magnetic Material Research Laboratory, Gandhi Institute of Technology and Management (GITAM) University Bengaluru, Karnataka, India
[d] Center for Advanced Materials (CAM), Qatar University, Doha 2713, Qatar
[e] Department of Biotechnology, GIT, GITAM (Deemed to be University), Visakhapatnam 530045, A.P., India
[f] Department of Clinical Chemistry, Faculty of Allied Health Sciences, Chulalongkorn University, Bangkok, 10330, Thailand
[g] Biosensors and Bioanalytical Technology for Cells and Innovative Testing Device Research Unit, Department of Clinical Chemistry, Faculty of Allied Health Sciences, Chulalongkorn University, Bangkok, 10330, Thailand
[h] Department of Physics, New Horizon College of Engineering, Bangalore 560103, India

ARTICLE INFO

Article history:
Received 31 December 2022
Revised 18 April 2023
Accepted 20 April 2023
Available online 24 April 2023

Keywords:
CO_2 hydrogenation
Methanol
Pd/CeO_2 nanorods
Tuning metal loading
Carbon neutral

ABSTRACT

One of the most significant industrial processes is the catalytic methanol synthesis from carbon dioxide because methanol is a future energy carrier for producing fuels and high-value-added commodities, the so-called "methanol economy" is carbon neutral. As a solution to climate change, the widespread belief that carbon dioxide can be recycled by hydrogenation into methanol has motivated the development of more efficient and selective catalysts. Efficient 2 wt% Pd/CeO_2 catalysts for thermochemical CO_2 hydrogenation have recently been investigated. However, the rationale behind the low Pd loading (2 wt%) in CeO_2 needs to be clarified, and comprehensive research into Pd tuning is lacking. In this article, we describe the synthesis ofvarious palladium contents (0.5, 1, 2, 4, and 6 wt%) supported on ceria nanorods (Pd/CeO_2) for selective hydrogenation of CO_2 to methanol under vapor-phase. The impact of Pd on the physicochemical properties of CeO_2 was examined using various characterization techniques. The enhanced catalytic activity was caused by the 2 wt% Pd/CeO_2 catalyst's most significant level of metallic Pd species, strong interactions between Pd and CeO_2, uniform Pd dispersion on CeO_2, increased reducibility, oxygen mobility, and weak basic sites. This study reveals that changing the percentage of metal in the catalyst supports a valuable technique for designing efficient oxides-supported metal-based catalysts for CO_2 conversions.

1. Introduction

Finding a way to mitigate climate change and temperature rise is one of humanity's most pressing challenges in the twenty-first century. The most significant greenhouse gases (GHGs) that contribute to global warming are carbon dioxide (CO_2), methane (CH_4), and nitrous oxide (N_2O), all of which are fluorinated gases. Approximately 79% of the greenhouse effect is attributed to CO_2, 11% to CH_4, 7% to N_2O, and 3% to fluorinated gases (O_3) [1]. Despite being the most abundant GHGs, water vapor acts as feedback of the greenhouse effect and varies with temperature. Instead, CO_2 is primarily to blame for the greenhouse effect. Due to the fact that CO_2 has a higher concentration in the atmosphere and a longer retention time than other GHGs [2]. Increases in the amount of CO_2 released into the atmosphere contribute to global environmental degradation. Scientists have become increasingly interested in finding ways to convert this potentially dangerous gas into value-added chemicals and industrial feedstocks as atmospheric CO_2 levels have steadily risen over the years. To meet this target by 2050, 7–32% of CO_2 emitted from the combustion of fossil fuels to generate electricity will need to be recycled [3]. From 1990 to 2050, the European Commission aims to reduce its energy-related CO_2 emissions by 80–95% [4].

Furthermore, initiatives to remove excess CO_2 from the atmosphere through capture and geological sequestration. These two approaches can be used on a large scale, but some drawbacks pre-

* Corresponding authors.
E-mail addresses: research.raaj@gmail.com (R. Boddula), noora.alqahtani@qu.edu.qa (N. Al-Qahtani).

https://doi.org/10.1016/j.mset.2023.04.006
2589-2991/

vent this. CO_2, the primary component of industrial waste gas, has numerous potential applications aside from its role as a GHG mitigation tool, including non-toxic, inexpensive, thermodynamically stable, inert, corrosion and fire resistant, and low-cost chemical feedstock for renewable fuels (e.g., methanol, ethanol, methane, dimethyl ether, formic acid, dimethyl carbonate, lower hydrocarbons, aromatics,). Thus, CO_2 utilization is one of the best alternative renewable sources to reduce GHG emissions and liberation from conventional sources such as petroleum, coal, and natural gas. As a result, converting CO_2 into economically viable fuels is a potentially game-changing approach to solving the energy problem and lowering the greenhouse effect. As a result, future CO_2 reduction targets will rely heavily on technologies that enable efficient CO_2 reuse in producing value-added chemicals or fuel products [2,5]. Catalytic hydrogenation is one method of utilizing CO_2. As a result, there is growing interest in using green hydrogen to convert CO_2 into more valuable chemicals or fuels [6–13].

Methanol (CH_3OH or MeOH) is a green liquid fuel and hydrogen transporter, as well as a raw material for the production of essential industrial chemicals and petrochemicals; therefore, research on its hydrogenation to methanol has been prioritized [14]. Commercially, methanol production increased by a factor of two from 2020 (157 MMT) to 2030 (311.4 MMT) [15]. Despite the fact that numerous electrochemical, photochemical, and photoelectrochemical pathways for CO_2 reduction are being investigated [16], it is more difficult to perform since it involves breaking high energy C=O bonds without any applied potential, and the realization of green chemistry's promise. The end products of CO_2 hydrogenation to methanol typically consist of CH_4 and CO compounds except for CH_3OH (equations (1)–(3)) [15]. Furthermore, it is thermodynamically preferred at low temperatures and high pressure since it is an exothermic reaction (equations (1) and (2)).

$$CO_2 + 3H_2 \leftrightharpoons CH_3OH + H_2O \;\; \Delta H_{298K} = -49.8 kJ/mol \tag{1}$$

$$CO_2 + 2H_2 \leftrightharpoons CH_3OH \;\; \Delta H_{298K} = -91.0 kJ/mol \tag{2}$$

$$CO_2 + H_2 \leftrightharpoons CO + H_2O \;\; \Delta H_{298K} = +41.2 kJ/mol \tag{3}$$

$$CO_2 + 4H_2 \leftrightharpoons CH_4 + 2H_2O \;\; \Delta H_{298K} = -164.7 kJ/mol \tag{4}$$

$$CH_4 + H_2O \leftrightharpoons CO + 3H_2 \;\; \Delta H_{298K} = -206.0 kJ/mol \tag{5}$$

Because of this trade-off, high CO_2 conversion typically results in lower methanol selectivity. Significant advancements have been made over the years in the chemical reduction of CO_2 in the presence of reducing agents over homogeneous and heterogeneous catalysts [17–22]. Modifying the reaction parameters, such as the temperature, pressure, and CO_2/H_2 ratio, allows one to fine-tune the product distribution and CO_2 conversion. This reaction is typically carried out at high pressure (>3 MPa) and moderate temperature (200–300 °C). Despite the progress that has been made in the hydrogenation of mixed syngas ($CO/CO_2/H_2$) over a commercial Cu-ZnO-Al_2O_3 catalyst to produce a low yield of methanol product due to the reverse water gas shift (RWGS) reaction (equation (3) [23]. Palladium (Pd) and its based bimetallic catalysts demonstrated superior activity (>10% CO_2 conversion) with 100% methanol selectivity over Cu-based catalysts, particularly at low pressure (3 MPa) and low temperature (250 °C) [11], The Cu sintering and the competing RWGS process reduces the catalyst lifetime and methanol selectivity. It is thus important to design catalysts that are both efficient and stable over time, allowing for the production of large quantities of methanol.

Catalytic conversion of CO_2 to methanol typically involves the two procedures below [24]: i) CO_2 adsorption, activation, and stabilization of activated intermediates the activated intermediates necessary for further hydrogenation to methanol instead of RWGS, and (ii) by dissociating the H-H bond in H_2 and encouraging reactions with the activated intermediates that yield methanol rather than other byproducts such as CH_4. Much research and development have been invested in discovering and perfecting extremely active and selective catalysts for the aforementioned reaction. Catalysts for CO_2 hydrogenation can be categorized into two categories such as metals (Rh, Re, Pt, Au, Cu, and Pd) based catalysts and oxide supports (ZnO, ZrO_2, Cr_2O_3, Ga_2O_3, In_2O_3, CeO_2, and Ga_2O_3-ZrO_2) [19,23,24]. Metals undergo reaction occurs at below 300 °C which is thermodynamically preferable for methanol production, whereas oxide-supports require extremely high reaction temperatures to dissociate H_2 over oxides. The favorable activation of CO_2 on oxide supports and the activation of H_2 on supported metals make oxide-supported catalysts attractive candidates for this reaction. Common mechanisms for the activity of these catalysts include the alloy produced at oxide-metal contacts and/or the robust metal-support interaction (MSI). Since the oxide support aids in enhancing metal dispersion, forming support-metal interfacial sites, and modifying surface properties via oxygen vacancy concentrations, basicity, and acidity, it plays a critical role in regulating catalytic activity [25].

Fan et al reported that 2 wt% Pd loading on CeO_2 catalysts with various morphologies (rods, cubes, and polyhedrons) were tested in the autoclave for the liquid-phase hydrogenation of CO_2 into formate [26] and that Pd/CeO_2 catalysts with rods morphology exhibited high catalyst activity. Similarly, Feng et al. studied 2 wt% Pd loading on CeO_2 catalysts with various morphologies (rods, cubes, octahedrons, and polyhedrons) for gas-phase hydrogenation of CO_2 into methanol [27]. It was found that CeO_2 rods with exposed (1 1 0) crystal facets are more active than CeO_2 octahedrons with exposed (1 1 1) crystal facets and CeO_2 cubes with exposed (1 0 0) crystal facets, which is attributed to the plentiful oxygen vacancies on the CeO_2 rods surface of Pd/CeO_2 catalyst. Further investigation into the effect of promoters (La, Zr, Cr, Ca, Co, Cd, Zn, Bi, and K) over Pd/CeO_2 catalysts revealed that the reactivity of oxygen vacancies is correlated with their formation energy [11]. This implies that a favorable oxygen vacancy formation energy may be advantageous for enhancing CO_2 reactivity. Pd (2 wt%) loadings and promoter (1 wt%) are constant. However, it is unclear and perflex why the nominal Pd loading in CeO_2 is only 2 wt%. There is also no information on how Pd loadings affect CeO_2 support and how this affects the activity and selectivity of CO_2 hydrogenation reactions. As a result, developing a highly-efficient Pd/CeO_2 nanorods catalyst system for CO_2 hydrogenation necessitates tuning the different wt% of Pd loadings on CeO_2 support. The goal of this study is to assess the effect of Pd loading on (1 1 1) crystal facets of CeO_2 nanorods support for catalytic CO_2 hydrogenation to methanol. Several techniques were used to determine how Pd influenced CeO_2's physicochemical properties. Separately, we investigated the catalytic properties of CO_2 hydrogenation and found that they have a structure–activity relationship.

2. Experimental

2.1. Preparation of catalysts

Porous nanorods were prepared [28] by dissolving 0.87 g of cerium nitrate in 10 ml deionized water and slowly mixing in 35 ml of sodium hydroxide (2.4 M) solution. They aged the mixture for 30 min before performing the reaction in the autoclave at 373 K for 24 h. The reaction mixture was then allowed to cool to room temperature (RT) before being collected the precursor products, which were centrifuged thoroughly washed in deionized water, and dried 383 K in the air. By subjecting this precursor to hydrothermal conditions, CeO_2 nanorods could be formed by heat-

ing this precursor solution to 433 K for 12 h. Synthesis of a series of Pd/CeO_2 catalysts with varying Pd loadings ranging from 0.5 to 6 (0.5, 1, 2, 4, and 6) wt% was enabled by wet-impregnation of palladium chloride [29] on the CeO_2 support. After a 12 h drying period at 383 K, the catalysts were calcined at 673 K for 4 h.

2.2. Characterization of catalysts

X-ray diffraction (XRD) tests were performed at 40 kV and 20 mA with a ramp rate of 2°/minute using nickel-filtered Cu Kα radiation. The rheological behavior of Pd-supported CeO_2 materials was studied employing N_2-adsorption–desorption isotherms at 77 K in a Micromeritics ASAP 2020 system. The catalysts were first evacuated for 3 h at 473 K. Transmission electron microscopy (TEM) images were captured using a Hitachi HT7700 instrument operating at 100 kV. The powder catalysts were dissolved in ethanol by sonication for 10 min, and the solution was diffused onto Cu grids in a sample holder placed in a microscope column. The Philips/Fei Quanta 200F scanning electron microscope (SEM) was used to take the SEM images, which were captured at 20 kV. Surface area and pore size were quantified using the Brunauer-Emmett-Teller (BET) and Barret-Joyner-Halenda (BJH) techniques. BET equation that is used to compute BET values. UV–Vis diffuse reflectance spectra (UV-DRS) were analyzed using the GBC UV–Visible Cintra instrument. The acidity of the catalysts was analyzed by using temperature-programmed desorption of CO_2 (CO_2-TPD) and temperature-programmed reduction of hydrogen (H_2-TPR) on a 2920 Micromeritics instrument. For the CO chemisorption experiment, 50 mg of calcined catalyst was loaded into a U-shaped quartz microreactor, followed by an in-situ reduction with 5% H_2/Ar (30 ml/minute) at 473 K for 1 h. Following that, a 1 h high-purity He (30 ml/minute) purge was performed at 473 K. After allowing it to cool to RT. The catalyst was exposed to a mixture for at least 20 pulses at 5% CO/He until no CO adsorption was observed. For the H_2-TPR experiment, 30 mg of calcined catalyst was placed in a U-shaped quartz microreactor, and the temperature and pressure were then heated at a rate of 373 K/minute under 5% H_2/Ar (30 ml/minute). The amount of hydrogen measured by thermal conductivity detector (TCD). Before taking a reading in a CO_2-TPD experiment, an in-situ reduction and oxidation reaction were performed on 100 mg of catalyst then purged He at 473 K for 1 h. Following sample cooling to RT exposed to high purity CO_2 (30 ml/minute) for another 1 h, and then purified by extreme precision. Finally, the acquired sample was heated at a rate of 278 K/minute in high purity He and CO_2 desorption signals were recorded while through a TCD detector.

2.3. Catalytic activity

Vapor phase hydrogenation of CO_2 for methanol synthesis was studied in a continuous fixed bed with a stainless-steel tube reactor operating at standard conditions (513 K and 3 MPa). To level out the temperature distribution, 0.3 g of Pd/CeO_2 catalyst was mixed with 1 g of quartz sand and packed into the reactor to level out the temperature distribution. The typical catalyst was first reduced in an H_2 flow of 30 ml/minute for 1 h at 873 K and 1 MPa. We fed reactants into the reactor (H_2/CO_2 ratio of 3), brought the reaction pressure up to the target value, and raised the temperature to the target value. Effluent products like CO_2, CH_4, and CH_3OH were analyzed using an online gas chromatograph with an autosampler and two detectors of TCD, and a flame ionization detector (FID) as well as N_2 as the internal standard. The reported values are based on the steady-state conditions attained after 6 h of reaction time. The below equation is used to calculate the selectivity of CH_3OH and CH_4 and the conversion of CO_2 calculated.

$$CO_2\ conversion\ (\%) = \frac{\text{molar flow of } CO_2\text{(inlet gas)} - \text{molar flow of } CO_2\text{(outlet gas)}}{\text{molar flow of } CO_2\text{(inlet gas)}} \times 100\%$$

$$Product\ selectivity\ (\%) = \frac{\text{molar flow of } one\ product\ (outlet\ gas)}{\text{molar flow of } all\ products\ (outlet\ gas)} \times 100\%$$

3. Results and discussion

3.1. Structure and composition of the catalysts

3.1.1. XRD

Fig. 1 depicts the XRD patterns of prepared pristine CeO_2 and various Pd/CeO_2 catalysts. All the samples exhibited the diffraction peaks at 28.55° (111), 33.05° (200), 47.59° (220), 56.32° (311), 59.14° (222), 69.39° (400), 76.64° (331), and 79.06° (420)) which are consistent with the fluorite-type oxide structure of CeO_2 phase (JCPDS No. 34–0394) [30]. The observed XRD pattern does not contain any peaks (especially, Pd (111) diffraction peak expected position at 35-45°) associated with any other crystalline PdO in all the samples up to 6 wt% Pd loading. The PdO species are obviously too small for XRD to detection limitation for XRD technique (their average size is < 4 nm) [31]. Thus, PdO particles are uniformly dispersed on CeO_2 support or Pd particles are integrated into the ceria lattice. Bera et al [32] found no evidence for the formation of PdO peaks at 5 wt% Pd/CeO_2 and only very weak peaks were noticed at 10 wt% Pd/CeO_2 upon calcining Pd/CeO_2 catalysts at 800 °C. The XRD analysis revealed no distinct peaks because PdO and CeO_2 support formed a mixed oxide phase, no distinctive peaks were seen in the XRD analysis. Priolkar et al. [33] also reported that formation of a solid solution between palladium particles and ceria on Pd/CeO_2 catalysts. Therefore, XRD results confirm that no distinct diffraction peaks of Pd are appeared due to the extremely dispersed Pd species inclusion into the CeO_2 for the formation of Pd_x-$Ce_{1-x}O_{2-\delta}$ solid solution [27].

3.1.2. BET surface area and pore-size distribution measurements

The results of nitrogen physisorption measurements on the specific surface areas of several Pd/CeO_2 catalysts are listed in Table 1. The BET surface area of pure CeO_2 was measured to be 49 m^2/g. Pd loading was found to have a negative effect on the specific surface area. Pore size distribution measurements provide evidence that this may be due to crystallites of palladium oxide fill-

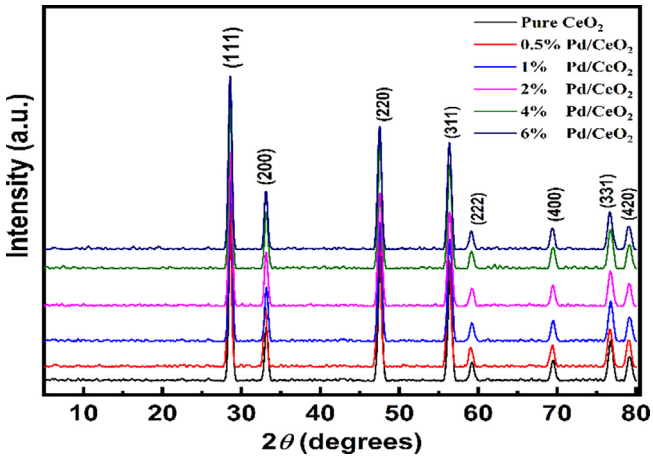

Fig. 1. XRD patterns of various pure CeO_2 and various Pd/CeO_2 catalysts.

Table 1
Textural properties of different Pd/CeO_2 catalysts.

Pd loading (wt%)	BET surface area (m^2 g^{-1})	Total pore volume (cm^3 g^{-1})	Total pore area (m^2/g)	Average pore diameter (Å)
0.0	49	0.31	87	138
0.5	39	0.29	85	137
1	31	–	–	–
2	30	0.25	71	145
4	31	–	–	–
6	21	0.24	80	124

ing up the support's pores or Pd species covering the CeO_2 support's surface. Mercury intrusion porosimetry has been used to measure the pore size distribution of a number of Pd/CeO_2 catalysts. Table 1 shows the results of measuring the average pore diameter, total pore area, and total pore volume of a variety of Pd/CeO_2 catalysts. As Pd loading rises, the catalyst's total pore volume, pore area, and pore diameter of the catalyst all decrease. The decrease in pore volume, pore area, and pore diameter observed with increasing Pd loading is most likely due to pore blockage and physical deposition of PdO on the support's surface.

3.1.3. CO chemisorption

Table 2 shows the Pd dispersion, metal area, and crystallite size calculated from the irreversible CO uptake values of various Pd/CeO_2 catalysts calcined at 773 K. The Pd concentration was determined to be between 88% and 15%. The material's high dispersion at low Pd loading may be due to Pd's strong interaction with oxygen-containing groups on the CeO_2 support. With increasing Pd content, deposition is more likely to occur on the outer surface of CeO_2 supports. As a result, agglomeration will be facilitated, reducing metal dispersion by shortening the distance between metallic species.

Increasing the Pd content on the support leads to an increase in Pd crystallites or agglomeration, as shown in Table 2. This reduces Pd dispersion and metal area. Pd crystallites may be less readily available for CO chemisorption as Pd metal content increases due to a decrease in surface area. The relationship between palladium loading and various physical properties is depicted in Fig. 2. The amount of CO chemisorbed Pd active sites, Pd density, and Pd metal surface area of the catalyst increase up to a Pd loading of 2 wt% and decrease at higher Pd loadings, as shown in Fig. 2. Higher Pd loadings result in a smaller metal area because fewer Pd active sites are available for CO adsorption. Findings from other characterizations that are reasonably consistent with CO chemisorption.

3.1.4. UV–Vis DRS

The UV–Vis diffuse reflectance spectra of various Pd/CeO_2 samples are shown in Fig. 3. The charge-transfer (CT) bands of Pd^{2+} ions provide information about their surroundings. The UV-DR spectrum of the Pd/CeO_2 catalysts revealed three adsorption bands: one at 240 nm, another at 280 nm, and a large one at 420 to 450 nm. The band at 240 nm is attributed to a ligand–metal charge transfer (LMCT of Pd ← O-Ce), which is typical of supported Pd catalysts, and the band at 280 nm is due to a metal–ligand charge

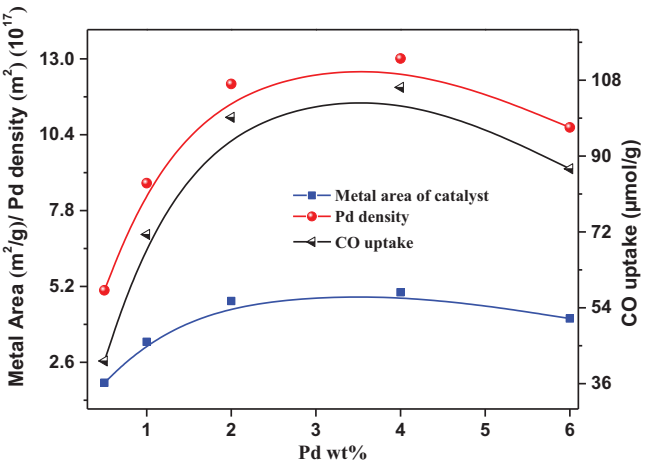

Fig. 2. Effect of metal loading on the metal surface area, Pd density, and CO uptake of various Pd/CeO_2 catalysts.

transition (MLCT of Ce-O ← Pd), as reported in the literature [34–36]. The band observed between 420 and 450 nm is attributed to d-d transitions of tetra-coordinated Pd^{2+} ions in an oxygen environment with D_{4h} symmetry [37]. The 240 and 280 nm bands show the formation of dispersed Pd species (Pd-O-Ce). These findings suggest that Pd^{2+} ions are either bound to the oxygen atoms on the surface of CeO_2 or have formed tiny PdO particles [35,36]. Assigning the broad adsorption band at 420–450 nm to the d-d transition of PdO is very exciting. This peak's strength at low Pd loadings suggests that PdO is in a highly dispersed amorphous state or that crystallites have small sizes. The d-d transition band shifts to a longer wavelength region as Pd loading increases, and its intensity increases. This data strongly suggests that increasing crystallite size or bulk PdO occurs at higher loadings. It is that as Pd loading increased, dispersion decreased because PdO particles on CeO_2 grew larger [36]. These findings provide strong evidence for the existence of two distinct environments for Pd species in the present catalytic system: one caused by dispersed palladium, and the other caused by bulk PdO.

3.1.5. H_2-TPR

The H_2-TPR analysis was performed to verify the reducibility of Pd species in Pd/CeO_2 catalysts with different Pd loading, and the results are shown in Fig. 4. H_2-TPR profile of pure CeO_2 shows

Table 2
Percentage dispersion, average particle size, metal surface area, and CO-uptake of various Pd/CeO_2 catalysts.

Pd loading (wt%)	Dispersion (%)	CO_{irr} uptake (µmol/g)	Metal area (m^2/g_{pd})	Crystallite size (nm)
0.5	88.2	41.4	392.9	1.27
1	75.9	71.4	338.5	1.47
2	52.8	99.2	235.1	2.12
4	28.3	106.3	125.9	3.96
6	15.4	87.0	68.7	7.26

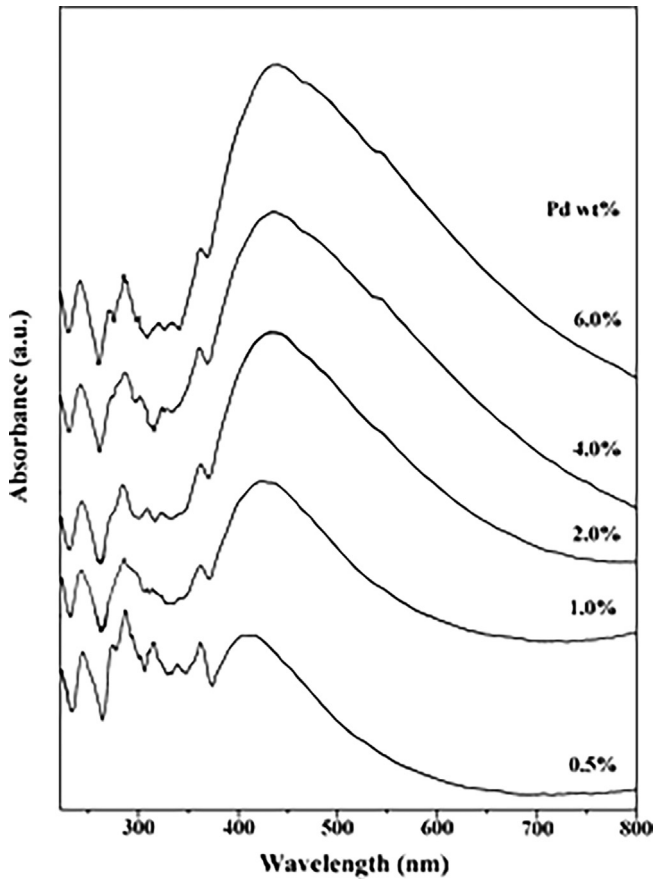

Fig. 3. UV–Vis diffuse reflectance spectra of various Pd/CeO_2 catalysts.

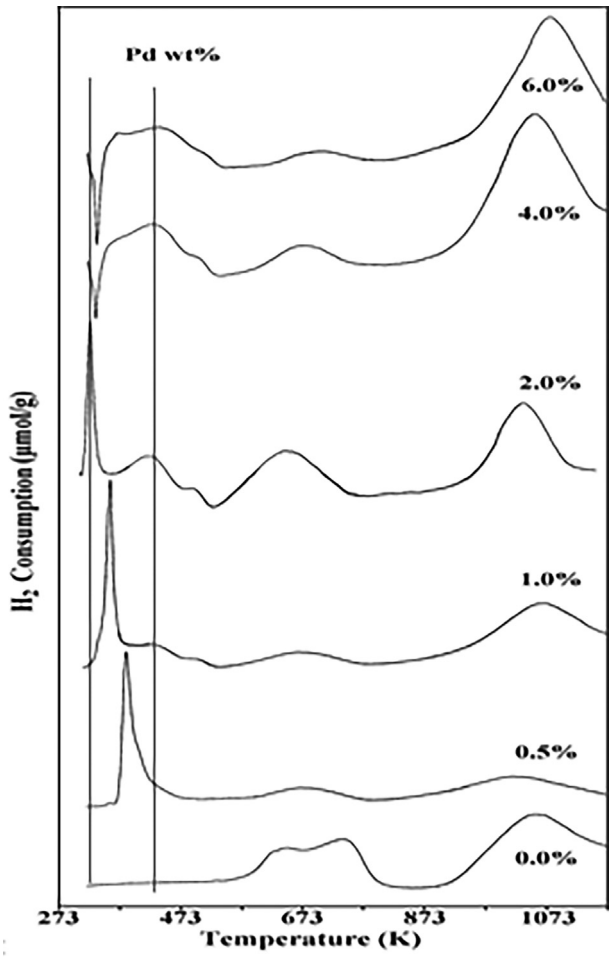

Fig. 4. H_2-TPR profiles of various Pd/CeO_2 catalysts.

two distinct reduction peaks at 737 and 1057 K, which are attributed to the removal of oxygen from the material's surface and bulk, respectively. This result corroborates improved robust MSI between Pd and CeO_2, as a result of a smaller average Pd particle size and an increase in the number of Pd(II) species in the Pd/CeO_2 catalyst, with outcomes resembling those of increased surface oxygen produced by reducing, the surface oxygen vacancies interact with Pd cations to form atomically distributed Pd species [27].

Different reduction profiles are observed for Pd/CeO_2 samples and it shows a high-intensity peak at a low-temperature peak (384–322 K) and a low-intensity peak at a high-temperature peak (430 K). The addition of Pd significantly altered the reduction behavior of ceria. CeO_2's Surface and bulk oxygen reduction peaks of CeO_2 shifted to lower temperatures. The low-temperature reduction peak is caused by larger particles or bulk PdO crystallites, which are unreacted with CeO_2. Dispersed Pd species on the support are responsible for the high-temperature reduction peak. As Pd loading increased, the low-temperature peak moved to a lower temperature region and vanished above 2 wt% Pd. The intensity of this peak increases until it reaches 1 wt% Pd, and then it gradually decreases as the Pd loading increases. The high-temperature peak is caused by tiny Pd particles (strong interaction with CeO_2) that are widely dispersed across the CeO_2 surface (430 K). It is well known that incorporating Pd in to ceria-related materials improves their reactivity towards reduction. The maximum peak at 737 K of pure CeO_2 support has shifted to a lower temperature region in the H_2-TPR of Pd/CeO_2 catalysts due to hydrogen spillover from metal to support. The ability of Pd to dissociate hydrogen activates oxygen species at the surface and bulk of ceria, facilitating their reducibility in Pd/CeO_2 catalysts at lower temperatures. However, the movement of the maximum peaks may be caused by the interaction of the strong metal and the support. The oxygen reduction is thought to take place solely at the metal and support surfaces. PdO to Pd° conversion always requires more hydrogen than is available (H_2/Pd > 1) (Table 3). Theoretically, hydrogen uptake of a Pd (1 wt%) based catalyst is close to 94 mol/g_{cat}, owing primarily to the reduction of Pd^{2+} sites [31]. The excess higher H_2 uptake is attributed to the reduction of surface as well as bulk CeO_2. The intensity of reduction peaks of CeO_2 support increases as Pd loading increases and also shifts to the higher temperature. These results clearly show that metal-support interaction decreased as metal loading increased, resulting in a decrease in support surface reduction. It is also clear that as Pd loading increases, some larger palladium crystallites form, which are likely to be reduced at ambient temperature during the TPR process. This is also one of the factors for low-intensity peaks at higher loadings. The TPR profiles of Pd/CeO_2 catalysts show the appearance of a sharp negative peak from 4 wt% Pd at around ~ 332 K, which strongly indicates the generation of hydrogen during the TPR. In this process, some of the H_2 molecules simultaneously dissociate on the Pd crystals to form an unstable β-Pd hydride phase. When the temperature is raised to 332 K, it releases molecular hydrogen, resulting in a sharp negative peak. As shown in Fig. 4, when Pd loading on CeO_2 increases, the negative peak intensity also increases because of the formation of larger Pd particles in the catalyst facilitating the formation of more β-PdH_x phase.

Table 3
H_2 consumption and reaction temperature of the various Pd/CeO_2 Catalysts from H_2-TPR profiles.

Pd loading (wt%)	T_{red1} (K) (Negative)	A	T_{red2} (K) (Positive)	B	T_{red3} (K)	C	T_{red4} (K)	T_{red5} (K)
0.0	–	–	–	–	–	–	737	1057
0.5	–	–	384	217.0	430	20.7	685	1050
1.0	–	–	357	239.3	430	29.8	679	1068
2.0	–	–	322	106.8	428	56.5	648	966
4.0	332	36.5	–	–	435	58.5	677	1062
6.0	333	64.3	–	–	444	60.4	696	1070

A = negative peak hydrogen consumption; B = positive peak (T_{red2}) hydrogen consumption; C = positive peak (T_{red3}) hydrogen consumption.

3.1.6. CO_2-TPD

CO_2-TPD was used to determine the basicity of Pd/CeO_2 catalysts (Fig. 5), which depicts four regions of varying basicity for Pd/CeO_2 catalysts. The desorption peak at 413 K could be attributed to weak basic sites, which are likely related to lattice bound –OH groups or surface hydroxyl groups. The medium basic sites are responsible for the peak at 573 K, which corresponds to the O groups, while the strong basic sites are responsible for the peak at 863 K, which corresponds to the O^{-2} and Pd^{+2} pairs. The peak above > 973 K is attributed to extremely strong basic sites caused by Pd and Ce cations. It is important to take into account the possibility of structural changes occurring on the catalysts when considering data obtained from CO_2 desorbed at temperatures above 973 K. Furthermore, the high-strength basic sites (T_D > 973 K) were not considered for discussion in this work because the cleaning step prior to CO_2 saturation was carried out at lower temperature. Table 4 lists the number of basic sites in terms of µmol/g CO_2 desorbed. Since CO_2 uptake increases as Pd loading increases, the Pd phase is primarily responsible for the catalyst's basicity. Pd-supported catalysts reveal that the concentration of weak basic sites increases up to a Pd loading of 2 wt% and then decreases. The decline in weak basicity with increasing Pd loadings could be attributed to the extent of Pd crystallites. The catalytic activity is caused by weak basic sites, according to experimental evidence [38]. These findings are supported by evidence from CO_2 hydrogenation, which shows that the conversion increases up to 2 wt% of Pd loading and then stabilizes at higher Pd loadings. This is more evidence that weak basic sites are helpful for CO_2 hydrogenation. A low CO_2 adsorption capacity on Pd species results in a high methanol selectivity on Pd/CeO_2 catalysts. Since CO_2 uptake increases with increased Pd loading, the Pd phase is primarily responsible for the basicity of catalysts due to the presence of a number of weak, medium, and strong basic sites.

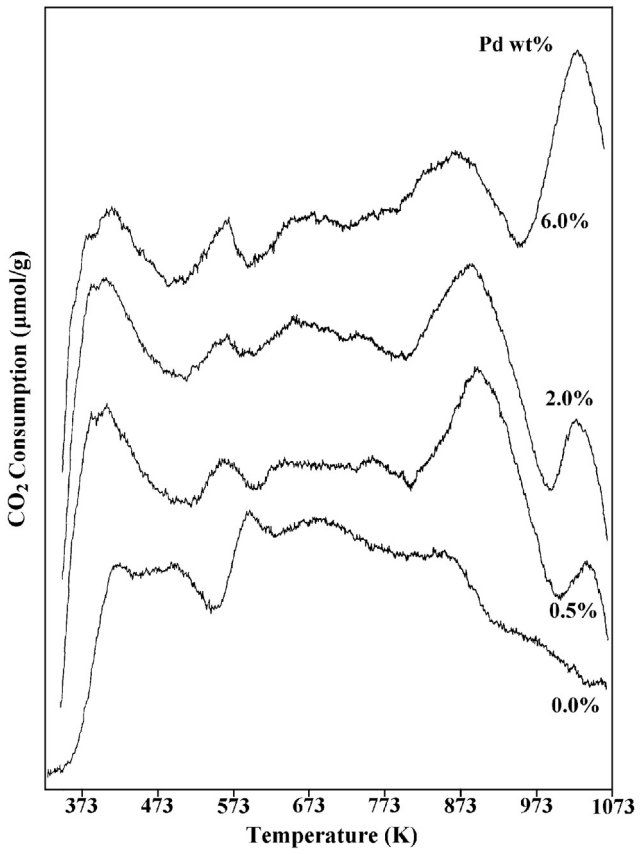

Fig. 5. CO_2-TPD profiles of selected Pd/CeO_2 catalysts.

3.1.7. Morphological study

The morphological investigations of pure CeO_2 and the most optimized catalyst, 2 wt% Pd/CeO_2 are shown in Fig. 6. These studies were conducted using electron microscopy (scanning electron microscopy (SEM) and transmission electron microscopy (TEM). Fig. 6. shows CeO_2 nanorods with dimensions of 50–150 nm in length as well as 10 nm in diameter. There are no Pd particles visible on the CeO_2 rods. This means that the Pd species are distributed uniformly across the CeO_2 surface.

3.2. Catalytic activity

The hydrogenation of CO_2 at 513 K was performed using various Pd/CeO_2 catalysts. A significant role was played over varying Pd loading on the CeO_2 support during the conversion of CO_2 and selectivity of methanol. Higher Pd loadings tended to decrease CO_2 conversion, while Pd loadings up to 2 wt% increased it. The crystallinity of Pd on the support may be responsible for a decrease in CO_2 conversion after 2 wt% of Pd. Based on similar experiments, pure CeO_2 was not able to hydrogenate CO_2. CO_2 hydrogenation activity, like CO chemisorption and catalyst area, has an interesting structure–activity relationship with Pd loading. If palladium is loaded to 2% wt, the catalyst becomes more exposed to metal atoms and has a larger surface area. Furthermore, Pd loading of up to 2% wt increased basic site strength. This increased strength decreased as Pd loadings increased. Based on these tests, the CO_2 conversion is precisely related to the number of active Pd sites and the basic strength of the catalyst.

Fig. 7 depicts an analysis of the relationship between CO_2 hydrogenation and Pd loading. TOF is expressed as the amount of CO_2 molecules transformed per unit time per Pd-exposed site. As illustrated in Fig. 7, A structure–activity relationship exists between Pd dispersion and CO_2 hydrogenation activity up to 2 wt% Pd loading, but the relationship becomes less significant beyond this loading. When the crystallite size of the Pd atom is changed, the per-site activity (TOF) changes significantly. This indicates that the reaction is extremely structure-sensitive. The high CO_2 hydrogenation activity appears at low Pd loadings due to max-

Table 4
CO_2-TPD of various Pd/CeO_2 samples.

Pd loading (wt%)	CO_2 uptake (μmol/g)				Total CO_2 uptake (μmol/g)
	weak	medium	strong	very strong	
0.0	57	45	74	–	176
1.0	119	100	152	84	455
2.0	123	102	133	144	502
6.0	102	112	116	249	579

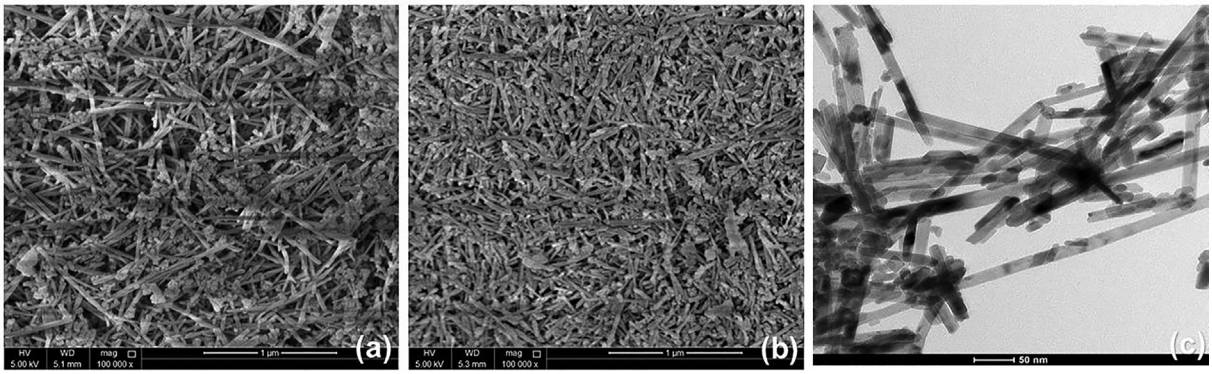

Fig. 6. SEM images of (a) pure CeO_2 and (b) 2 wt% Pd/CeO_2 and its TEM image (c).

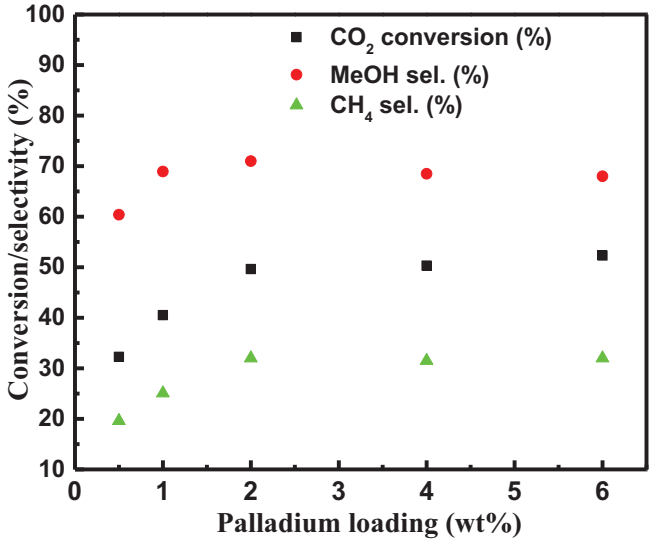

Fig. 7. Hydrogenation of CO_2 over various Pd/CeO_2 catalysts.

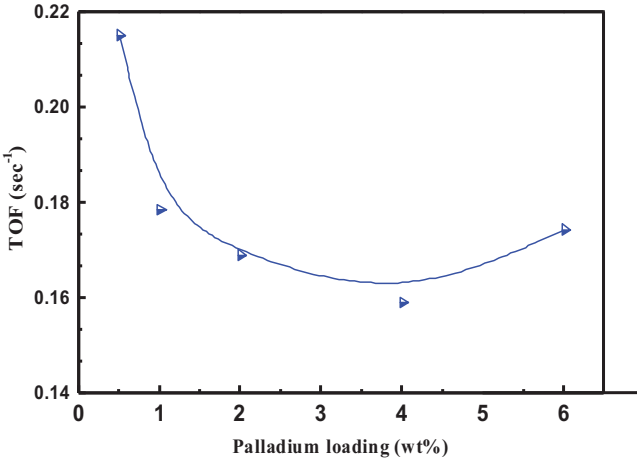

Fig. 8. TOF vs. Pd% loading in various Pd/CeO_2 catalysts.

imum Pd metal dispersion, whereas at higher Pd loadings, the activity is invariably due to Pd crystallization. As expected, the catalytic results agree well with those obtained by dispersion and other techniques.

The influence of reaction temperature on CO_2 hydrogenation over 2 wt% Pd/CeO_2 and the results were shown in Fig. 8. At a low reaction temperature of 473 K, the 2 wt% Pd/CeO_2 catalyst showed 20.4% CO_2 conversion and 61.7% MeOH selectivity. As the reaction temperature raised from 473 K to 513 K, the CO_2 conversion improved from 20.4 to 49.6% and the MeOH selectivity increased from 61.7 to 71%. As the reaction temperature increased to 533 K, the conversion of CO_2 increased to 55.3%, while the selectivity of MeOH decreased to 60.5% with an increase in methane selectivity. This means that higher temperatures promote the formation of methane and the CO_2 conversion to paraffins. Considering these results, the reaction temperature of 513 K is revealed to be the optimum temperature for the best CO_2 conversion and MeOH selectivity.

2 wt% Pd/CeO_2 catalyst tested for the CO_2 hydrogenation on various reaction pressures and the results were shown in Fig. 9. Under a relatively low reaction pressure of 1 MPa, the CO_2 conversion rate was 41.6%, the MeOH selectivity was 65.0% and the methane selectivity was 22%. As the reaction pressure increased from 1 MPa to 3 MPa, the conversion of CO_2 increased to 49.6%, the MeOH selectivity increased slightly to 71%, and the methane selectivity increased to 29%. As the reaction pressure further raised from 2 MPa to 5 MPa, the CO_2 hydrogenation decreased to 45.6% and the selectivity of MeOH also decreased to 68.4%. Therefore, according to the obtained results, confirmed that the 2 wt% Pd/CeO_2 exhibited the best catalytic performance at a moderate reaction pressure of 3 MPa.

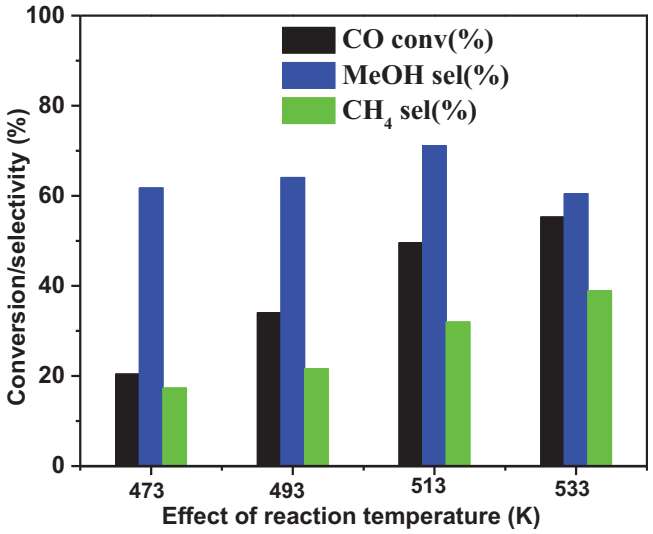

Fig. 9. Effect of reaction temperature on CO_2 hydrogenation over 2 wt% Pd/CeO_2 catalyst.

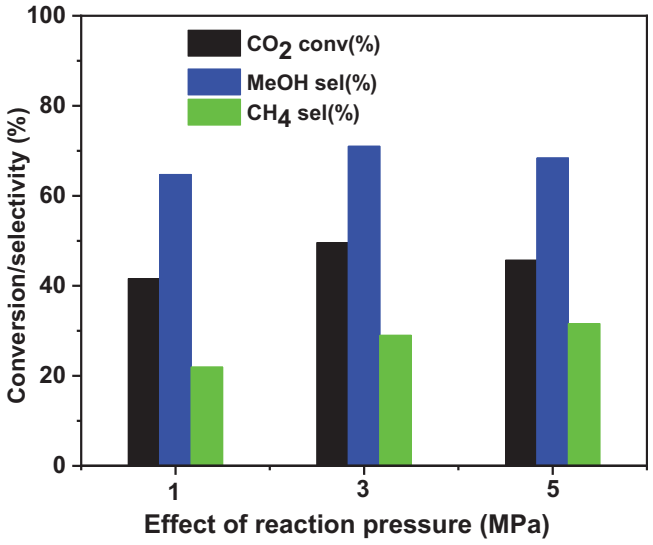

Fig. 10. Effect of reaction pressure on CO_2 hydrogenation over 2 wt% Pd/CeO_2 catalyst.

Fig. 10 shows the influence of GHSV (3000–4200 ml· g^{-1}·h^{-1}) on the hydrogenation of CO_2 over 2 wt% Pd/CeO_2 catalyst. At a low GHSV of 3000 ml $g^{-1}h^{-1}$, CO_2 conversion was 49.6%, MeOH selectivity was 69.5% and methane selectivity was 30.6%. As the GHSV flow rate increased, the CO_2 conversion decreased to 48.7%, while the MeOH selectivity decreased slightly to 29.1%. Further increasing the GHSV to 4200 ml·g^{-1}·h^{-1} resulted in decline in conversion of CO_2 to 47.2% and a slight decrease in MeOH selectivity upto 68.6%. From the above results, it can be seen that higher CO_2 conversion was obtained at lower GHSV 3000 ml·g^{-1}·h^{-1}, which may be due to longer contact time between the CO_2 and H_2 feed gas mixture with the catalyst, thus enhancing the catalytic activity. As the GHSV rate increases, CO_2 conversion decreases, mainly because the retention time of CO_2 on the catalyst surface is too short for the reaction. Among these results, GHSV 3600 ml·g^{-1}·h^{-1} is best for CO_2 conversion and high MeOH selectivity (see Fig. 11).

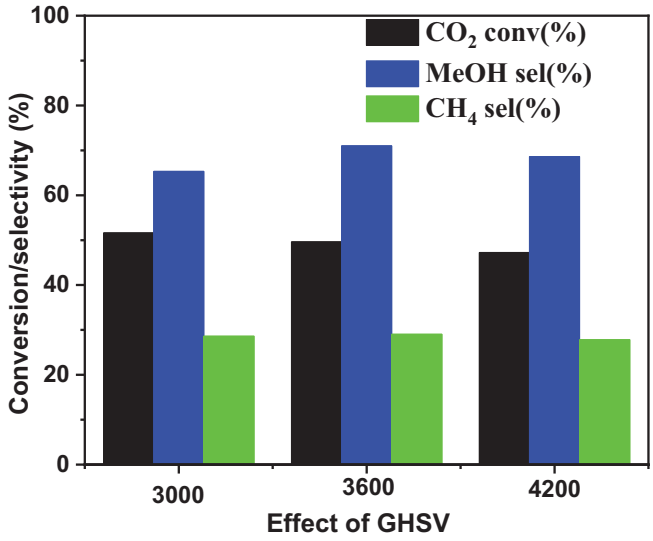

Fig. 11. Effect of GHSV on CO_2 hydrogenation over 2 wt% Pd/CeO_2 catalyst.

4. Conclusions

In conclusion, wet-impregnation of CeO_2 nanorods with varying Pd loadings (0, 0.5, 1, 2, 4, and 6 wt%) followed by annealing resulted in the successful fabrication of Pd/CeO_2 catalysts. The XRD results for Pd-loaded CeO_2 nanorods showed (1 1 1) crystal facets of CeO_2 with no evidence of Pd-based phases. The pore blockage and physical deposition of PdO on the support surface contribute to the decrease in pore volume, pore area, and pore diameter observed with increasing Pd loading, resulting in a BET surface area of approximately 30 m^2/g for the 2 wt% Pd/CeO_2 nanorods, which is significantly lower than that of as-synthesized CeO_2 nanorods (49 m^2/g). Based on the data, the most effective catalyst exhibited the following properties: a surface area of 30 m^2/g; a pore volume of 0.25 cm^3/g; a metal area of 235.1 m^2/g; a Pd dispersion of 52.8%; a CO_{irr} uptake and basic site activity of 99.2 μmol/g; 502 μmol/g. According to the H_2-TPR findings, Pd addition can greatly increase its reducibility and activity of the catalyst. It has been proven by transmission electron microscopy that Pd is uniformly distributed on CeO_2 nanorods, and that increasing oxygen mobility can boost catalytic activity. Excellent selectivity for methanol from gas-phase CO_2 hydrogenation was observed using a 2 wt% Pd/CeO2 nanorods catalyst thanks to the robust MSI between Pd and CeO_2 nanorods resulting to a smaller average Pd particle size and an increase in the number of Pd(II) species, increased surface oxygen produced by reducing, the surface oxygen vacancies interact with Pd cations to form atomically distributed Pd species. This study demonstrates a structure–activity correlation between catalyst structure, composition, particle size, reducibility, and basicity and CO_2 hydrogenation catalytic activity in different wt% Pd loading on CeO2 catalysts.

CRediT authorship contribution statement

Ramyakrishna Pothu: Conceptualization, Methodology, Investigation, Supervision, Writing – review & editing, Writing – original draft. **Harisekhar Mitta:** Data curation. **Prasun Banerjee:** Data curation. **Rajender Boddula:** Conceptualization, Methodology, Investigation, Supervision, Writing – review & editing, Writing – original draft. **Rajesh K. Srivastava:** . **Pramod K. Kalambate:** Software, Validation. **Ramachandra Naik:** . **Ahmed Bahgat Radwan:** Software, Validation. **Noora Al-Qahtani:** Funding acquisition.

Declaration of Competing Interest

The authors declare that they have no known competing financial interests or personal relationships that could have appeared to influence the work reported in this paper.

Acknowledgements

This work was supported by Qatar University through a National Capacity Building program Grant (NCBP), [QUCP-CAM-20/23-463]. Statements made herein are solely the responsibility of the authors.

References

[1] C.H. Tan, S. Nomanbhay, A.H. Shamsuddin, Y.K. Park, H. Hernández-Cocoletzi, P.L. Show, Current Developments in Catalytic Methanation of Carbon Dioxide—A Review, Front. Energy Res. 9 (2022), https://doi.org/10.3389/fenrg.2021.795423.

[2] Neeraj, S. Yadav, Yadav, Carbon storage by mineral carbonation and industrial applications of CO_2, Mater Sci Energy Technol. 3 (2020) 494–500.

[3] R. Guil-López, N. Mota, J. Llorente, E. Millán, B. Pawelec, J.L.G. Fierro, R.M. Navarro, Methanol Synthesis from CO_2: A Review of the Latest Developments in Heterogeneous Catalysis, Materials. 12 (2019) 3902, https://doi.org/10.3390/ma12233902.

[4] M. Takht Ravanchi, S. Sahebdelfar, Catalytic conversions of CO_2 to help mitigate climate change: Recent process developments, Process Saf. Environ. Prot. 145 (2021) 172–194, https://doi.org/10.1016/j.psep.2020.08.003.

[5] A.S. Malik, S.F. Zaman, A.A. Al-Zahrani, M.A. Daous, Turning CO_2 into di-methyl ether (DME) using Pd based catalysts – Role of Ca in tuning the activity and selectivity, J. Ind. Eng. Chem. 103 (2021) 67–79, https://doi.org/10.1016/j.jiec.2021.07.019.

[6] S. Dey, G.C. Dhal, Materials progress in the control of CO and CO_2 emission at ambient conditions: An overview, Mater Sci Energy Technol. 2 (2019) 607–623, https://doi.org/10.1016/j.mset.2019.06.004.

[7] M. Zhang, M. Wu, Z. Wang, R. Cheng, D.Y.C. Leung, Z. Lu, S.P. Feng, Efficient sunlight driven CO_2 reduction on Graphene-wrapped Cu-Pt/rTiO_2@SiO_2, Mater Sci Energy Technol. 3 (2020) 734–741, https://doi.org/10.1016/j.mset.2020.09.001.

[8] K. Sun, Z. Zhang, C. Shen, N. Rui, C. Liu, The feasibility study of the indium oxide supported silver catalyst for selective hydrogenation of CO_2 to methanol, Green, Energy Environ. 7 (2022) 807–817, https://doi.org/10.1016/j.gee.2021.05.004.

[9] X. Yang, J. Cheng, X. Yang, Y. Xu, W. Sun, J. Zhou, MOF-derived Cu@Cu_2O heterogeneous electrocatalyst with moderate intermediates adsorption for highly selective reduction of CO2 to methanol, Chem. Eng. J. 431 (2022), https://doi.org/10.1016/j.cej.2021.134171 134171.

[10] H. Song, A. Fazeli, H.D. Kim, A. Alizadeh Eslami, Y.S. Noh, N. Ghaffari Saeidabad, D.J. Moon, Effect of lanthanum group promoters on Cu/(mixture of ZnO and Zn-Al-spinnel-oxides) catalyst for methanol synthesis by hydrogenation of CO and CO_2 mixtures, Fuel 283 (2021), https://doi.org/10.1016/j.fuel.2020.118987 118987.

[11] F. Jiang, F. Jiang, S. Wang, Y. Xu, B. Liu, X. Liu, Catalytic Activity for CO_2 Hydrogenation is Linearly Dependent on Generated Oxygen Vacancies over CeO_2-Supported Pd Catalysts, ChemCatChem 14 (2022), https://doi.org/10.1002/cctc.202200422 e202200422.

[12] T. Guo, Q. Guo, S. Li, Y. Hu, S. Yun, Y. Qian, Effect of surface basicity over the supported Cu-ZnO catalysts on hydrogenation of CO_2 to methanol, J. Catal. 407 (2022) 312–321, https://doi.org/10.1016/j.jcat.2022.01.035.

[13] O.A. Ojelade, S.F. Zaman, A review on CO_2 hydrogenation to lower olefins: Understanding the structure-property relationships in heterogeneous catalytic systems, J. CO2 Util. 47 (2021), https://doi.org/10.1016/j.jcou.2021.101506 101506.

[14] J. Fernández-González, M. Rumayor, A. Domínguez-Ramos, A. Irabien, Hydrogen Utilization in the Sustainable Manufacture of CO_2 -Based Methanol, Ind. Eng. Chem. Res. 61 (2022) 6163–6172, https://doi.org/10.1021/acs.iecr.1c04295.

[15] E.J. Choi, Y.H. Lee, D.W. Lee, D.J. Moon, K.Y. Lee, Hydrogenation of CO_2 to methanol over Pd–Cu/CeO2 catalysts, Molecular, Catalysis. 434 (2017) 146–153, https://doi.org/10.1016/j.mcat.2017.02.005.

[16] T. Biswal, K.P. Shadangi, P.K. Sarangi, R.K. Srivastava, Conversion of carbon dioxide to methanol: A comprehensive review, Chemosphere 298 (2022) 134299.

[17] S.F. Zaman, O.A. Ojelade, H. Alhumade, J. Mazumder, H.O. Mohamed, P. Castaño, Elucidating the promoting role of Ca on PdZn/CeO_2 catalyst for CO_2 valorization to methanol, Fuel 343 (2023), https://doi.org/10.1016/j.fuel.2023.127927 127927.

[18] A.S. Malik, S.F. Zaman, A.A. Al-Zahrani, M.A. Daous, H. Driss, L.A. Petrov, Selective hydrogenation of CO_2 to CH_3OH and in-depth DRIFT analysis for PdZn/ZrO_2 and CaPdZn/ZrO_2 catalysts, Catal. Today 357 (2020) 573–582, https://doi.org/10.1016/j.cattod.2019.05.040.

[19] O.A. Ojelade, S.F. Zaman, A Review on Pd Based Catalysts for CO_2 Hydrogenation to Methanol: In-Depth Activity and DRIFTS Mechanistic Study, Catal. Surv. Asia 24 (2020) 11–37, https://doi.org/10.1007/s10563-019-09287-z.

[20] O.A. Ojelade, S.F. Zaman, M.A. Daous, A.A. Al-Zahrani, A.S. Malik, H. Driss, G. Shterk, J. Gascon, Optimizing Pd: Zn molar ratio in PdZn/CeO_2 for CO_2 hydrogenation to methanol, Appl. Catal. A 584 (2019), https://doi.org/10.1016/j.apcata.2019.117185 117185.

[21] A.S. Malik, S.F. Zaman, A.A. Al-Zahrani, M.A. Daous, H. Driss, L.A. Petrov, Development of highly selective PdZn/CeO_2 and Ca-doped PdZn/CeO_2 catalysts for methanol synthesis from CO_2 hydrogenation, Appl. Catal. A 560 (2018) 42–53, https://doi.org/10.1016/j.apcata.2018.04.036.

[22] O.A. Ojelade, S.F. Zaman, CO_2 Hydrogenation to Methanol over PdZn/CeO_2 Catalyst, Academic Publishing House (2019), https://doi.org/10.7546/CRABS.2019.06.05.

[23] P. Gao, L. Zhang, S. Li, Z. Zhou, Y. Sun, Novel heterogeneous catalysts for CO_2 hydrogenation to liquid fuels, ACS Cent. Sci. 6 (2020) 1657–1670, https://doi.org/10.1021/acscentsci.0c00976.

[24] K. Li, J.G. Chen, CO_2 Hydrogenation to Methanol over ZrO_2-Containing Catalysts: Insights into ZrO_2 Induced Synergy, ACS Catal. 9 (2019) 7840–7861, https://doi.org/10.1021/acscatal.9b01943.

[25] P. Ebrahimi, A. Kumar, M. Khraisheh, A Review of CeO_2 Supported Catalysts for CO_2 Reduction to CO through the Reverse Water Gas Shift Reaction, Catalysts 12 (2022) 1101, https://doi.org/10.3390/catal12101101.

[26] L. Fan, J. Zhang, K. Ma, Y. Zhang, Y.-M. Hu, L. Kong, A.-P. Jia, Z. Zhang, W. Huang, J.-Q. Lu, Ceria morphology-dependent Pd-CeO_2 interaction and catalysis in CO_2 hydrogenation into formate, J. Catal. 397 (2021) 116–127, https://doi.org/10.1016/j.jcat.2021.03.025.

[27] F. Jiang, S. Wang, B. Liu, J. Liu, L. Wang, Y. Xiao, Y. Xu, X. Liu, Insights into the Influence of CeO_2 Crystal Facet on CO_2 Hydrogenation to Methanol over Pd/CeO_2 Catalysts, ACS Catal. 10 (2020) 11493–11509, https://doi.org/10.1021/acscatal.0c03324.

[28] S. Zhang, Z.Q. Huang, Y. Ma, W. Gao, J. Li, F. Cao, L. Li, C.R. Chang, Y. Qu, Solid frustrated-Lewis-pair catalysts constructed by regulations on surface defects of porous nanorods of CeO_2, Nat. Commun. 8 (2017), https://doi.org/10.1038/ncomms15266.

[29] R. Pothu, N. Mameda, R. Boddula, H. Mitta, V. Perugopu, N. Al-Qahtani, Sustainable conversion of biodiesel-waste glycerol to acrolein over Pd-modified mesoporous catalysts, Mater Sci Energy Technol. 6 (2023) 226–236, https://doi.org/10.1016/j.mset.2022.12.012.

[30] M. Wu, M. Miao, W. Li, X. Zhang, L. Zhang, T. Zhen, Y. Fu, J. Jin, L. Yuan, Metal-organic framework-derived one-dimensional Pd@CeO_2 catalysts with enhanced activity for methane oxidation, Fuel 331 (2023) 125575.

[31] H. Zhu, Z. Qin, W. Shan, W. Shen, J. Wang, Pd/CeO_2–TiO_2 catalyst for CO oxidation at low temperature: a TPR study with H_2 and CO as reducing agents, J. Catal. 225 (2004) 267–277, https://doi.org/10.1016/j.jcat.2004.04.006.

[32] P. Bera, K.C. Patil, V. Jayaram, G.N. Subbanna, M.S. Hegde, Ionic Dispersion of Pt and Pd on CeO_2 by Combustion Method: Effect of Metal-Ceria Interaction on Catalytic Activities for NO Reduction and CO and Hydrocarbon Oxidation, J. Catal. 196 (2000) 293–301, https://doi.org/10.1006/jcat.2000.3048.

[33] K.R. Priolkar, P. Bera, P.R. Sarode, M.S. Hegde, S. Emura, R. Kumashiro, N.P. Lalla, Formation of $Ce_{1-x}Pd_xO_{2-\delta}$ Solid Solution in Combustion-Synthesized Pd/CeO_2 Catalyst: XRD, XPS, and EXAFS Investigation, Chem. Mater. 14 (2002) 2120–2128, https://doi.org/10.1021/cm0103895.

[34] J.M.D. Cónsul, C.A. Peralta, E.V. Benvenutti, J.A.C. Ruiz, H.O. Pastore, I.M. Baibich, Direct decomposition of nitric oxide on alumina-modified amorphous and mesoporous silica-supported palladium catalysts, J. Mol. Catal. A Chem. 246 (2006) 33–38, https://doi.org/10.1016/j.molcata.2005.10.011.

[35] F.B. Noronha, D.A.G. Aranda, A.P. Ordine, M. Schmal, The promoting effect of Nb2O5 addition to Pd/Al_2O_3 catalysts on propane oxidation, Catal. Today 57 (2000) 275–282, https://doi.org/10.1016/S0920-5861(99)00337-5.

[36] R.S.G. Ferreira, P.G.P. de Oliveira, F.B. Noronha, Characterization and catalytic activity of Pd/V_2O_5/Al_2O_3 catalysts on benzene total oxidation, Appl Catal B 50 (2004) 243–249, https://doi.org/10.1016/j.apcatb.2004.01.006.

[37] Z. Boukha, M. Kacimi, M. Ziyad, A. Ensuque, F. Bozon-Verduraz, Comparative study of catalytic activity of Pd loaded hydroxyapatite and fluoroapatite in butan-2-ol conversion and methane oxidation, J. Mol. Catal. A Chem. 270 (2007) 205–213, https://doi.org/10.1016/j.molcata.2007.01.048.

[38] W. Liao, C. Tang, H. Zheng, J. Ding, K. Zhang, H. Wang, J. Lu, W. Huang, Z. Zhang, Tuning activity and selectivity of CO_2 hydrogenation via metal-oxide interfaces over ZnO-supported metal catalysts, J. Catal. 407 (2022) 126–140, https://doi.org/10.1016/j.jcat.2022.01.037.